AIAA JOURNAL
Vol. 33, No. 4, April 1995

Interaction of Jet Noise With a Nearby Panel Assembly

J. L. McGreevy*
Philadelphia College of Pharmacy and Science, Philadelphia, Pennsylvania 19104
A. Bayliss†
Northwestern University, Evanston, Illinois 60208
and
L. Maestrello‡
NASA Langley Research Center, Hampton, Virginia 23681

A model of the interaction of the noise from a spreading subsonic jet with a panel-stringer assembly is studied numerically in two dimensions. The radiation resulting from this flow/acoustic/structure coupling is computed and analyzed in both the time and frequency domains. The jet is initially excited by a pulse-like source inserted into the flowfield. The pulse triggers instabilities associated with the inviscid instability of the jet mean flow shear layer. These instabilities in turn generate sound which provides the primary loading for the panels. The resulting structural vibration and radiation depends strongly on panel placement relative to the jet/nozzle configuration. Results are obtained for the panel responses as well as the transmitted and incident pressure. The effect of the panels is to act as a narrow filter, converting the relatively broadband forcing, heavily influenced by jet instabilities, into radiation concentrated in narrow spectral bands.

Nomenclature

A = panel centered at the jet exit
B = panel located downstream of the jet exit
c_v = specific heat per unit volume
c_∞ = ambient speed of sound
D = width of jet nozzle
D_b = stiffness of the beam $Mh^3/12(1-\nu^2)$
E = total energy per unit volume
f = time dependent pulse
g = Gaussian function
h = beam thickness
M = modulus of elasticity
N_x = coefficient of nonlinear term in beam equation, defined by Eq. (2)
p = pressure
R = gas constant
$\hat{s}_1$ = starter pulse defined by Eq. (5)
T = temperature
t = time
U_J = jet exit velocity
U_0 = spreading jet profile
u = jet axial velocity component
v = tangential velocity component
x = axial coordinate centered at the horizontal location of the nozzle exit
y = tangential coordinate centered at the vertical location of the rigid wall
z = beam transverse deflection
γ = physical damping of the beam
ϵ = amplitude of the starter pulse
ν = Poission ratio of the beam
ρ = density
ρ_b = mass per unit volume of the beam

Subscripts

$+$ = reference to the location of the wall boundary from the side opposite the domain containing the jet
$-$ = reference to the location of the wall boundary from the domain containing the jet
x = derivative with respect to x
y = derivative with respect to y
t = derivative with respect to t
∞ = reference to ambient quantities

I. Introduction

IN this paper we study numerically the interaction between jet noise with a flexible aircraft-type structure. This interaction is important because the resulting panel vibration can result in both structural fatigue of the panel and increased interior noise levels. Although there have been previous studies of jet noise without the presence of the panels and studies of panel response to prescribed loading, the use of a fully coupled flow/structure/acoustics model is an essential prerequisite to a full understanding of panel response in the presence of jet noise.

There have been many important studies of the different sources of jet noise and their role on sound radiation. One formulation of the sources of jet noise was developed in the Lighthill acoustic analogy.[1] The resulting model led to scaling arguments for the dependence of the far-field sound on jet velocity, although the actual sources had to be modeled for calculation purposes. An independent theory of sound radiation, using a different formulation of the sources, was obtained in Ref. 2. Extensions of this work to account for shear interaction terms and vortical flows followed.[3–5]

An important consideration, particularly in subsonic jets, is the role of fluid dynamical instability waves as sources of jet noise. Experiments have demonstrated the existence of large-scale structures or instability waves in jets.[6–9] These structures are believed to act as sources of sound, a point also confirmed by analytical studies[10–15] and computations.[8,16–18] In general, the computation of jet noise from first principles is beyond the capabilities of most present day computers, and modeling must be employed to allow more efficient computation of the jet noise.

Various approaches have been employed to determine the panel response to jet noise or to other sources which can not be easily calculated. The sources in the flowfield can be taken from experimental measurements, (e.g., Refs. 19 and 20) or can be modeled using appropriate simplifications (e.g., Refs. 21 and 22). In the former case,

Received June 9, 1994; revision received Oct. 27, 1994; accepted for publication Oct. 31, 1994.

*Assistant Professor, Department of Mathematics and Physics.
†Professor, Deptartment of Engineering Sciences and Applied Mathematics.
‡Senior Staff Scientist. Associate Fellow AIAA.

the panel response could then itself be measured experimentally as in Ref. 23 or computed via solution of the resulting panel equation from the measured sources as in Refs. 19 and 20. Although experiments[23] in supersonic jets have succeeded in isolating features of panel response due to oscillating shocks and jet instabilities in general, the use of experimental measurements dictates that all physical mechanisms associated with the jet noise be intertwined, thus making it difficult to ascertain the role of individual physical mechanisms of jet noise on panel response. The alternative is to analytically model the sources of sound in the jet. This necessarily involves significant simplifications of an extremely complex phenomena, namely the generation and propagation of noise, and also typically does not account for the full fluid/acoustic/structure coupling of the panel response.

For sources that can be well approximated by modes of the panel, simple normal mode analysis suggests that the displacement would exhibit spectral peaks near the resonant frequencies of the panel, i.e., the natural frequencies. Even for such sources, other quantities such as the velocity and the radiated pressure, which must be obtained from solution of the wave equation (either fully coupled to the panel motion as done here or a posteriori using the uncoupled panel velocity as a boundary condition), will not necessarily exhibit spectral peaks at the natural frequencies. The spectrum of these quantities will depend on both the details of the forcing function and on the parameters of the panels. When the incident pressure is jet noise, as considered here, the situation is yet more complicated as the sources will be convecting downstream with the flow and may not be well approximated by modes of the panel. In this case even qualitative details of panel response would require a specification of the sources which accounts for the relevant features of jet noise generation.

In the present work, we study numerically the interaction of jet noise, emanating from a high subsonic jet, with a flexible aircraft-type structure. The emphasis is on 1) the role of sound generated from spatially growing instability waves associated with the jet shear layer as an excitation mechanism for the structural vibration, 2) the resulting vibration of and radiation from the panel assembly due to flow/acoustic/structure coupling, and 3) the effect of the placement of the panels, relative to the jet/nozzle configuration, on panel response and radiation.

We employ a computational model which accounts for the full coupling between the panel and the surrounding fluid. The computational domain includes the panels, the jet domain, in which acoustic disturbances are generated via a pulse starter, and a radiation domain, in which acoustic disturbances from the vibrating panels propagate (see Fig. 1). As a result of the pulse, an initial acoustic disturbance is generated. This acoustic disturbance propagates into the far field while undergoing convection and dispersion due to the flowfield. More importantly, the initial disturbance triggers the development of an instability wave, i.e., a large-scale structure which is slowly convected downstream along the jet axis, due to interaction with the unstable jet shear layer. This instability wave, which is qualitatively similar to structures observed in real jets,[6–9] is an important source of jet noise, as it triggers the development of other instability waves in a continuous fashion long after the initial disturbance due to the pulse has propagated away from the flowfield and the panels. We concentrate on the long time behavior of the excited jet, i.e., the behavior of unsteady disturbances in the jet long after the initial disturbance generated by the pulse has propagated from the region of interest.

The use of the pulse starter allows the qualitative simulation of instability wave generated sound in a spreading jet nonetheless sufficiently reducing the computational requirements so that high-resolution computations of the fully coupled flow/acoustic/structure interaction can be readily obtained. In particular, the model allows the direct computation of the sources of jet noise, the instability waves, together with the propagation of the resulting sound. The model also allows simulation of the dispersive effects such as the frequency dependent refraction of sound by the flowfield. This methodology is similar to that employed in Refs. 8, 11, and 16, where the direct computation of sources and sound propagation was studied for axisymmetric jets (without any nearby structure). These results demonstrated that the starter pulse was effective as a computational tool to excite instability wave generated sound and to study the bending (refraction effect) of sound waves through the jet flowfield. The results also demonstrated that the instability wave generated sound was highly directional, peaking at low to midangles from the jet axis and was concentrated at low frequencies.

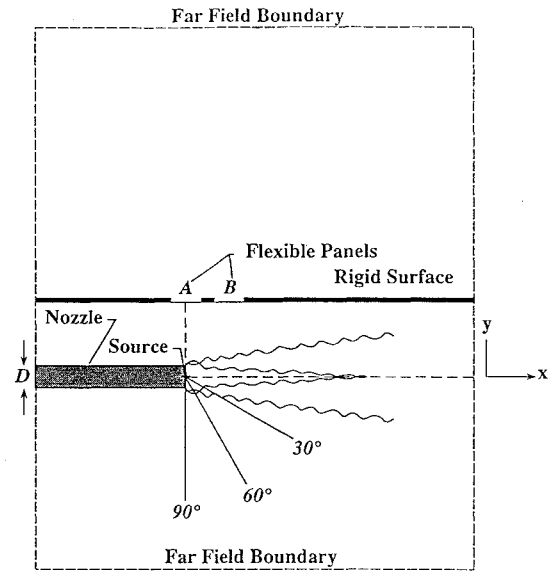

Fig. 1 Computational domain.

The sound from the sources we have computed leads to enhanced low-frequency vibration and radiation from the panels. The effectiveness of jet instabilities in exciting the panels is highly dependent on the placement of the panel relative to the jet exit. The panel acts as a narrow filter in converting a relatively broadband forcing field, heavily influenced by jet instabilities, into a relatively discrete vibration and radiation spectrum. The resulting radiation is beamed primarily in the vertical and downstream directions. Whereas the precise frequencies of the radiation will depend on the details of the flowfield and the mechanism of exciting the jet shear layer instabilities, we believe that the numerical computations presented here are a step in determining the role of jet noise excitation in exciting vibration and radiation from nearby surfaces.

In Sec. II we describe the model and the resulting numerical method. In Sec. III we illustrate the numerical validity of our computations and describe our results. In Sec. IV we summarize our conclusions.

II. Problem Formulation

The computational domain is shown in Fig. 1. Fluctuating pressure, density, and velocities are computed in two domains, that which contains the jet, exiting from a nozzle of width D, and the domain on the other side of the wall boundary. We will refer to the two domains as the jet and radiation domains, respectively. The wall boundary is a rigid wall containing two adjacent flexible panels (denoted A and B in Fig. 1) with rigidly clamped boundaries. The panels vibrate in response to excitation from jet noise and radiate sound into both domains. We focus primarily on acoustic radiation into the radiation domain, as the radiation into the jet domain is small compared to the large disturbances already present in the jet.

The numerical method involves coupling the computation of a nonlinear equation governing the panel responses (the beam equation) to an Euler computation performed in both the jet and radiation domains. The panel vibration is fully coupled to the fluid dynamics in that at each time step the pressure difference across the panels, computed from the Euler computations, serves as a forcing term for the beam equation. Similarly, the displacement obtained from the beam equation is differentiated in time and is imposed as a boundary condition for the Euler computations. The only approximation made is that of small displacement relative to the acoustic wavelength (e.g., Euler grid size) so that in the Euler code the panel location is taken as the horizontal line $y = 0$.

The nonlinear beam equation is given by

$$D_b \frac{\partial^4 z}{\partial x^4} - N_x \frac{\partial^2 z}{\partial x^2} + \rho_b h \frac{\partial^2 z}{\partial t^2} + \gamma \frac{\partial z}{\partial t} = p^+ - p^- \qquad (1)$$

The coefficient N_x of the nonlinear term is given by

$$N_x = \frac{Mh}{2L} \int_{x_0}^{x_0+L} \left(\frac{\partial z}{\partial x} \right)^2 dx \qquad (2)$$

which represents the tension created by the stretching of the plate due to bending. The pressures in the radiation and jet domains are p^+ and p^-, respectively. The solution of Eq. (1) is obtained at each time step using an implicit finite difference method developed in Ref. 24 coupled with Newton's method to account for the nonlinear term N_x. The panels are assumed clamped at both ends.

The coupling of the panel computation to the Euler computation occurs through the forcing term given on the right-hand side of Eq. (1). The pressures p^+ and p^- are obtained from the Euler computation which uses an explicit scheme. At each new time level p^+ and p^- are obtained by extrapolation of the pressure from the interior. The displacement at the new time level is then obtained by solving Eq. (1) one time step. Upon differentiating z, an approximation to the normal velocity is then obtained and employed as a boundary condition to complete the update to the Euler computation. Since this procedure is followed at each time step, the fluid and structural calculations are fully coupled. A detailed step-by-step procedure which describes the coupling is given below.

The Euler equations are solved in conservation form. In terms of the vector

$$\hat{w} = (\rho, \rho u, \rho v, E)^T$$

the equations can be written in the form

$$\hat{w}_t + \hat{F}_x + \hat{G}_y = 0 \qquad (3)$$

with the flux functions $\hat{F}$ and $\hat{G}$ given by

$$\hat{F} = [\rho u, \rho u^2 + p, \rho uv, u(E + p)]^T$$

$$\hat{G} = [\rho v, \rho vu, \rho v^2 + p, v(E + p)]^T$$

respectively. Here, u and v are the x and y components of the velocity, respectively, and

$$E = \tfrac{1}{2}\rho(u^2 + v^2) + c_v \rho T$$

The pressure p is obtained from the equation of state

$$p = \rho RT$$

The Euler equations (3) are solved separately in both the jet and radiation domains. We do not distinguish the vector w in each domain for clarity.

In the jet domain the Euler equations are modified to account for the jet flow. We assume a straight pipe of width D from which the jet exits. The solution is computed both within and exterior to the pipe, with rigid boundary conditions imposed on each side of the pipe. The system (3) is modified to account for two different source terms

$$\hat{w}_t + \hat{F}_x + \hat{G}_y = \hat{s}_1(t, x, y) + \hat{s}_2(x, y) \qquad (4)$$

The source term,

$$\hat{s}_1(t, x, y) = \epsilon f(t) g(x, y) \hat{w}_I \qquad (5)$$

serves as the starter pulse to excite the jet. Here, ϵ describes the amplitude of the source, $f(t)$ is a pulse which describes the time dependence of the source, and $g(x, y)$ determines the spatial distribution of the source. We take

$$g(x, y) = \exp(-\sigma^2 r^2)$$

where

$$r^2 = (x - x_s)^2 + (y - y_j)^2$$

is the distance from the source location (x_s, y_j), y_j is the location of the jet axis (approximately $6D$ from the wall), and x_s is approximately $1.2D$. To simulate a localized source we take $\sigma^2 = 1000D^2$. For the temporal dependence of the source we take

$$f(t) = \exp(-at^2 - b/t^2) \qquad (6)$$

The vector $\hat{w}_I$ is given by

$$\hat{w}_I = \left(1, U_0, 0, \frac{\gamma}{\gamma - 1} p_\infty\right)^T$$

where $U_0(x, y)$ is a model describing a spreading jet profile taken from Ref. 25 in Cartesian coordinates. This vector is chosen as follows. The component in the continuity equation serves as a mass injection. This is balanced by the component in the energy equation so that in the absence of flow and boundaries the solution remains homentropic. The component of the source in the axial momentum equation ensures that momentum is added to the system as the mass injected is convected downstream of the flow. In the absence of flow and bounding surfaces, the solution would be a circular wave. As part of the validation of the numerical scheme, the computation with no flow has been extensively checked by grid refinement to give a circular wave.

The second source term $\hat{s}_2(x, y)$ is designed so that in the absence of the starter pulse, i.e., $\epsilon = 0$, the solution to Eq. (4) would be a stationary profile corresponding to a spreading jet. The specified solution is

$$\hat{w}_0 = \left(\rho_\infty, \rho_\infty U_0, 0, \rho_\infty U_0^2/2 + c_v T_\infty\right)^T$$

In the limit of small ϵ, the effect of the source term $\hat{s}_2$ leads to the Euler equations linearized about a spreading jet, as in Refs. 8 and 17, which by itself need not be a solution to the Euler equations. Incorporation of this term within the nonlinear Euler equations allows for the computation of nonlinear disturbances within the mean jet profile as in Ref. 16. The inclusion of this source term separates the computation of the disturbance, in particular the resulting instability waves, from the computation of the mean flow (i.e., the spreading jet). Thus, the resulting system of equations allows for the simulation of instability waves and the resulting sound generation, together with the bending of acoustic waves in the jet flowfield without requiring the computation of the spreading jet itself. Although this is a simplified model, the resulting system simulates many of the observed features of instability wave generated jet noise and permits high resolution computation of the coupling of jet noise with the flexible panels and the resulting radiation from the panels.

The initial conditions are taken to be the mean state $\hat{w}_0$ in the jet domain and ambient data in the radiation domain. The panels vibrate in response to excitation by sound from the jet as they would in an aircraft on the ground since the mean state corresponds to a static jet. Both the jet domain and the radiation domain are, in principle, unbounded regions. These domains are closed by the imposition of nonreflecting boundary conditions at the far-field boundaries, indicated in Fig. 1. At these boundaries, we impose conditions designed to absorb outgoing circular waves.[26] Specifically we assume that the pressure has the functional form

$$p(t, x, y) \simeq h(c_\infty t - r, \theta)/\sqrt{r} \qquad (7)$$

where x and y are expressed in polar coordinates r and θ from a specified origin. Differentiation of Eq. (7) with respect to t and r results in the relation

$$p_t + c_\infty p_r + (p - p_\infty)/(2r) = O(r^{-3/2}) \qquad (8)$$

Neglecting the right-hand side of Eq. (8) results in a radiation boundary condition which is effective in simulating outgoing waves provided the boundaries are sufficiently distant from all sources. We

have verified that there are negligible boundary reflections for the data presented in this paper.

The Euler equations are solved using an explicit finite difference scheme which is fourth-order accurate in the spatial coordinates and second-order accurate in time. The scheme is a generalization of the second-order MacCormack scheme to allow higher order accuracy in space.[27] The numerical method has been validated on other problems of spatial instability. In particular, in Ref. 28 it was shown that the use of fourth-order differencing can lead to a dramatic improvement in the calculation of growth rates for spatially unstable disturbances. In the numerical method we employ operator splitting in the two coordinate directions. The scheme is discussed in detail in other publications.[8,17]

The fluid dynamics and structural dynamics are coupled via the boundary conditions on the panels. To clarify the nature of the coupling, we describe the steps involved in advancing the solution one time step.

1) Equations (3) are advanced one time step in both the jet domain and radiation domain. Boundary conditions are not imposed, however, temporary variables on the boundaries are obtained using third-order extrapolation of the flux functions as in Ref. 28. We note that in the jet domain, Eq. (3) is solved in both the interior and exterior of the pipe (see Fig. 1).

2) Using the temporary boundary values, the pressure difference across the panels is computed.

3) Equation (1) is advanced one time step using the computed pressure difference across the panels as a source term. This equation is formulated numerically so as to solve for the difference between the new and old beam acceleration.

4) The normal velocity on the panels is computed by integrating the acceleration.

5) The computed normal velocity is then used as a boundary condition for Eq. (3), for both the jet domain and the radiation domains.

6) The remainder of the boundary conditions for the jet domain and radiation domain are imposed. This includes imposition of the condition $v = 0$ on the rigid extensions of the panel, Eq. (8) on the artificial boundaries to simulate outgoing radiation, $v = 0$ on the inner and outer surfaces of the pipe, and characteristic conditions at the inflow pipe boundary (see Fig. 1). It is shown in Ref. 8 that characteristic conditions account for the lowest propagating mode within the pipe.

7) Go back to step 1 to update to the next time level.

III. Results

We consider a configuration as indicated in Fig. 1. The jet exits from a straight nozzle of width $D = 2$ in., assumed rigid on both the interior and exterior sides. The jet starter pulse (6) is located in the potential core at approximately $1.15D$ downstream of the nozzle exit on the axis of the jet. The constants a and b in Eq. (6) are $a = 3.4(c_\infty/D)^2$ and $b = 380(c_\infty/D)^{-2}$, chosen to give a frequency spectrum for f' within the range of interest for subsonic jets (the peak frequency is very close to 1000 Hz). An infinite wall is located approximately $6D$ above the jet and parallel to the nozzle. The wall is assumed rigid, except for two regions where flexible, aluminum, aircraft-type panels (panel A and panel B) with clamped boundaries are located. The panels are of length $5D$, thickness $0.01D$ and are centered at $x = 0D$ and $x = 5.24D$, respectively. Other parameters of the panels are typical of aluminum. The origin of coordinates is chosen to be the horizontal location of the nozzle exit for x and the vertical location of the rigid wall for y. For the computations described subsequently, we assume an exit flow Mach number of 0.65, with exit velocity $U_J = 0.65\, c_\infty$. Ambient conditions are assumed for ρ and p. Both the jet and radiation domains extend $48D$ downstream from $x = 0$, $12D$ in the upstream direction and $48D$ in the y direction. There are no detectable reflections from the artificial boundaries for the data presented here. We employ a grid of 511×351 points in the jet domain and 361×301 points in the radiation domain. The grid in the jet domain is stretched to improve resolution of the jet shear layer and source region.

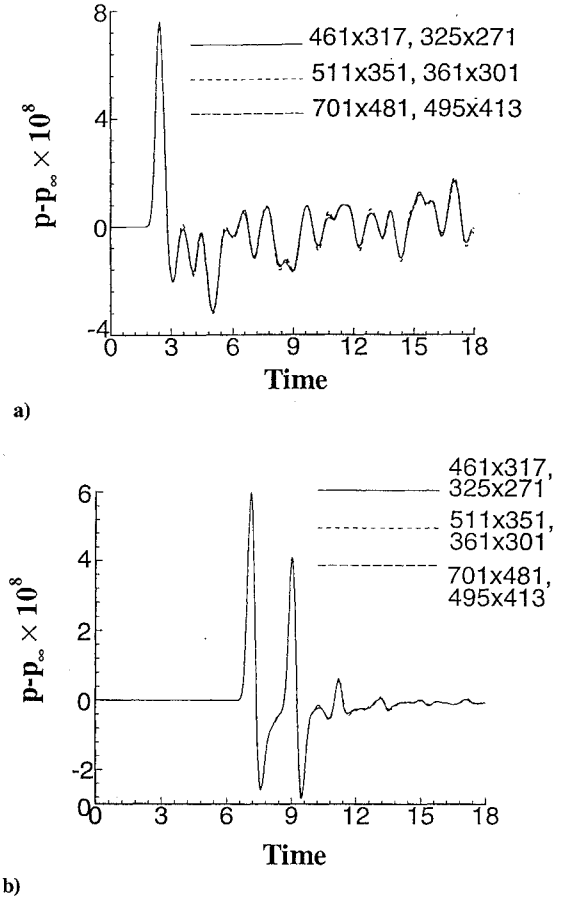

Fig. 2 Mesh refinements showing pressure-time histories: a) nearfield point at the center of panel A and b) farfield point on a circle of radius $r = 20D$ at 60 deg.

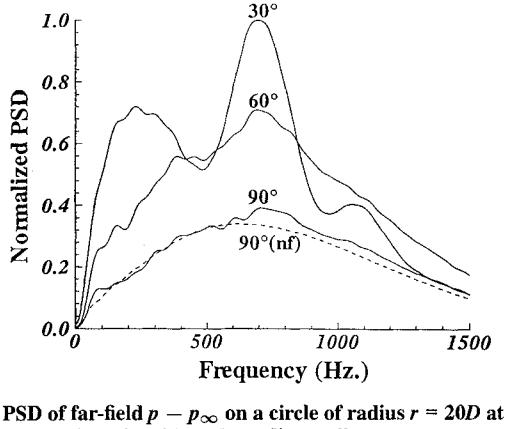

Fig. 3 PSD of far-field $p - p_\infty$ on a circle of radius $r = 20D$ at 30, 60, and 90 deg in a domain with no bounding walls.

Our results are presented in four parts; validation, the jet domain including the flow and acoustic radiation from the jet, the responses of the panels, and the acoustic radiation from the panels.

A. Validation

The numerical results were validated by mesh refinement. Preliminary validations included verifying that the solution was essentially omnidirectional if the flow and all bounding surfaces were removed. In addition, we verified that the solution at the locations considered here, as well as at other locations, was unaffected by changing the location of the artificial boundaries.

In Figs. 2a and 2b the results of grid refinements are shown. These figuresshow a comparison of pressure time histories for the

grid employed in the present work with coarser and finer grids. Two spatial points were tested, one in the near field, at the center of panel A, and one in the far field at $36D$ and 30 deg from the nozzle exit. Since the computation was in Cartesian coordinates, we chose the grid point that was closest to the selected radius and angle. The figures indicate that there are no visible effects of grid resolution within a range of grid sizes around the grid employed in this paper.

B. Jet Flow Domain

Nonstationary behavior in the jet is triggered by the pulse starter, which generates a disturbance that propagates through the jet, interacts with the shear layer, and then propagates into the far field as sound. In the far field this initial disturbance is noncircular due to convection. As a result of the interaction of the acoustic disturbance with the shear layer gradient of the mean jet profile, instability waves are created. This was shown in Ref. 29, in the context of a linearization of Eq. (3). These waves are inviscid, a consequence of the fact that the Euler equations are employed in the computation. The instability waves propagate longitudinally along the jet at speeds less than the speed of sound, spreading transversally as does the mean flow. After an initial growth, their amplitude decays with the velocity as the jet spreads. As they propagate downstream they act as sources of additional disturbances, as described in Refs. 1–3 and 13–15, which propagate into the far field as sound and also serve to excite further instability waves in the jet. This behavior is also consistent with experimental observations and with previous linear and nonlinear computations in Refs. 8 and 16. The resulting sound radiation forces the panels into a broadband response and radiation. The acoustic radiation persists after the initial disturbance generated by the pulse starter has propagated a significant distance from the panels and away from the region of interest.

Figure 3 shows power spectral densities (PSDs) of the far-field pressure ($36D$ from the nozzle exit) for the case of a domain without any bounding wall at 30, 60, and 90 deg. To facilitate comparison between the different angles, the data are normalized by the maximum PSD over all three angles. In addition, to clarify the effects of

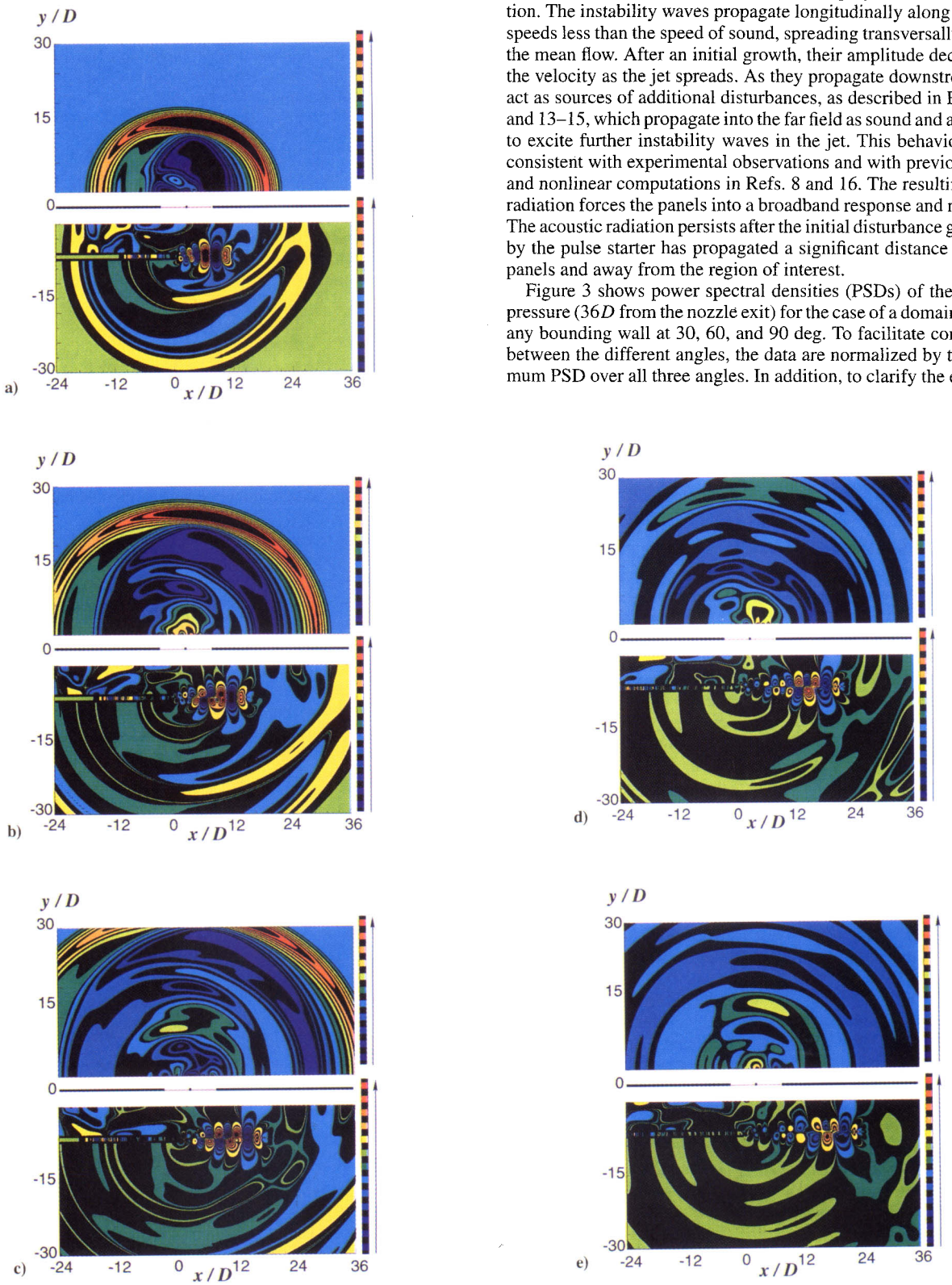

Fig. 4 Contours of constant $p - p_\infty$: a) time $t = 27.9D/c_\infty$, b) time $t = 38.4D/c_\infty$, c) time $t = 45.3D/c_\infty$, d) time $t = 62.8D/c_\infty$, and e) time $t = 73.3D/c_\infty$.

the flow, the figure also includes the results for a computation without any flow (but with a nozzle) at 90 deg (normalized by the same factor as the data with flow). We note that the no-flow computation is not quite omnidirectional due to scattering from the nozzle. We have verified that in the absence of the nozzle the no-flow computation is omnidirectional to a high degree of accuracy. This figure illustrates the role of the jet as an amplifier of sound. The acoustic far field is least affected by the flow for angles near 90 deg, a result also demonstrated in Ref. 8. The data at 30 deg shows two peaks, one near 700 Hz and another near 220 Hz. The 700-Hz peak corresponds to the peak frequency of the pulse, amplified due to the presence of flow as indicated by the large difference with respect to the no-flow case. The 220-Hz peak results primarily from the shear noise generated from flow instabilities. Such a behavior was also observed in Refs. 8 and 16 for axisymmetric jets. Low-frequency peaks are also observed at 60 deg, although the amplitudes are reduced with respect to the pronounced low-frequency peak at 30 deg. This figure illustrates that the computed sound radiation has features consistent with experimental observations.

The behavior of the resulting pressure field in the presence of the bounding wall, both within and outside of the flow, as well as the resulting acoustic radiation from the panels, is shown in Figs. 4a–4e for successive values of time. Note that although both the jet and radiation domains in the computation extend $48D$ in y, the figures show solutions extended only to $30D$ in y to expand the visualization of the acoustic field. In interpreting these figures, note also that the actual levels assigned to each color for the jet and radiation domain differ so that different colors are assigned to the ambient regions. However, for each domain the field values associated with any particular color is the same for all of the figures. The pressure level in the radiation domain ranges from -1.7×10^{-8} to 2.6×10^{-8} whereas the pressure level in the jet domain ranges from -4.0×10^{-6} to 4.1×10^{-6}. The relation between the colors and numerical values is indicated by the arrow on the right of each figure.

Figure 4a shows pressure contours at $t = 27.9D/c_\infty$, indicating the initial development of the unsteady jet flow and acoustic field of the jet and structure. There is a leading acoustic wave which propagates outside of the jet toward the far field and toward the wall, as well as upstream (both inside and outside the nozzle). As the leading wave reaches the wall, it reflects back and crosses the shear layer, trailing the initial disturbance, as shown in the figure. A large-scale structure, related to the spatial instability of the jet shear layer is generated along the jet exit. This structure slowly propagates downstream. As a result of the interaction between the flexible panels with the pulse, the resulting vibration creates an acoustic disturbance which propagates into the radiation domain. In the jet flowfield, as the disturbance evolves, additional instability waves are created behind the initial leading wave. These waves can be observed near the nozzle exit. The pressure field is clearly asymmetric about the jet axis due to the presence of the wall.

As time evolves (Fig. 4b) additional pressure waves are created from the jet instability wave which propagate into the far field. Figures 4b–4e show the evolution of the instability wave as it propagates downstream. The additional sound generated from this large-scale structure can also be seen by following the progression of the leading acoustic wave in Figs. 4b–4d. Although the initial waves due to the starter pulse exit the computational domain (Fig. 4d), additional instability waves continue to be generated within the jet shear layer, together with the associated shedding of acoustic disturbances from the nozzle lip. Hence, long after the initial waves generated by the pulse starter have propagated far downstream from the region of interest, indeed, after they have exited the domain, disturbances are continually generated which result in a continual excitation of the panels. In addition, Figs. 4a–4e show waves propagating between the pipe and wall boundary, upstream of the nozzle exit. The behavior just described has also been verified by a detailed animation of successive contours generated by the computation.

In Fig. 5 we illustrate the shedding of disturbances from the nozzle lip. The figure shows the pressure in a small region around the nozzle lip for three closely spaced values of time. In the top illustration, corresponding to the earliest time, the formation of a pressure disturbance at the upper lip of the nozzle exit can be seen. The middle illustration, at a slightly later time, shows that this disturbance has shed from the upper lip, whereas a new disturbance is being generated at the lower lip. In the bottom illustration, the disturbance has shed from the lower lip, whereas a new disturbance is forming at the upper lip. The figure illustrates the alternating shedding of pressure disturbances from both sides of the nozzle. This behavior is consistent with experimental observations[30] and is a source of sound forcing the panels to vibrate. A similar phenomenon was found in the axisymmetric computations[17] where ring type of disturbances were shed from the nozzle lip. The figures also illustrate the propagation of disturbances up the pipe.

C. Responses of the Panels

We first examine the panel response by examining the normal velocity, $v(x, t)$. In Figs. 6a and 6b we plot $v(x, t)$ over panels A and B, respectively, for nondimensional times ranging from $t = 7.2$ to $t = 10.2$. These times are after the primary excitation due to the pulse starter has occurred and include times when the panel is excited by sound emanating from instability waves in the flow.

The responses of the two panels are very different because of their locations. Panel A (Fig. 6a) is centered directly over the nozzle exit. As a result, it is excited by reflections between the pipe and the panel, together with the upstream and downstream propagation of sound from the jet. These two mechanisms give rise to a combination of standing waves and convecting waves on the panel. Over the interval $7 \leq t \leq 9$, the panel response is that of a standing wave which we believe is due to the multiple reflections between the wall and the pipe. For $9 \leq t \leq 10.2$, there are distinct propagating waves along the panel, propagating both upstream and downstream, which we believe originate with sound generated by the instability wave in the jet.

In contrast, panel B (Fig. 6b), which is located downstream of the nozzle exit, is excited primarily by convective disturbances generated by instabilities in the flow. The panel response is dominated by convective waves. The convective waves along the panel propagate in both the downstream and upstream directions, presumably due to reflections from the clamped ends of the panel. Waves propagating in both directions are indicated by the lines sketched on the figure. The speed of propagation of the convective wave is approximately $0.2c_\infty$, close to the speed of propagation of the instability waves. We emphasize that the panels are identical in all respects and that the different responses are a consequence of their location relative to the nozzle exit.

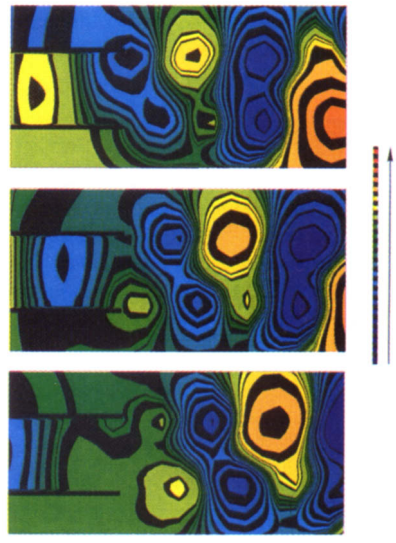

Fig. 5 Evolution of pressure disturbances shed from the nozzle lip at three successive times (from top to bottom) $t = 34.9D/c_\infty$, $t = 36.6D/c_\infty$, $t = 38.4D/c_\infty$; expanded region about the nozzle lip.

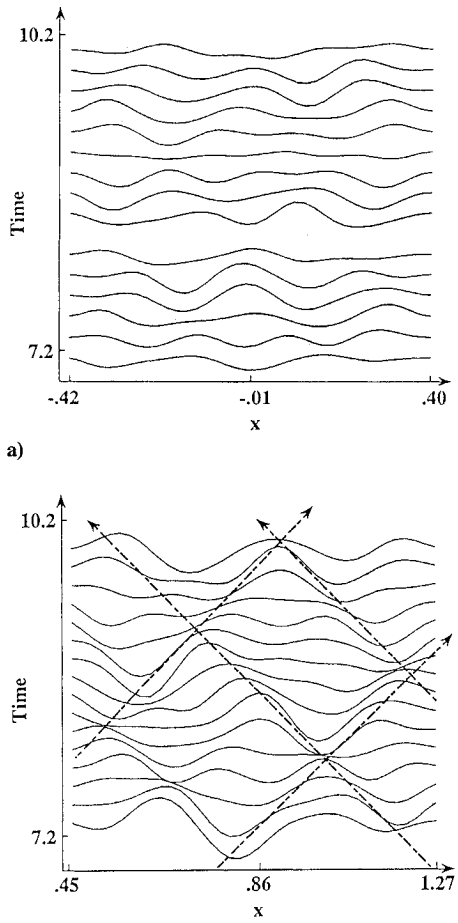

Fig. 6 Spatial plots of $v(x, t)$ for times ranging from $t = 7.2$ to $t = 10.2$: a) panel A and b) panel B.

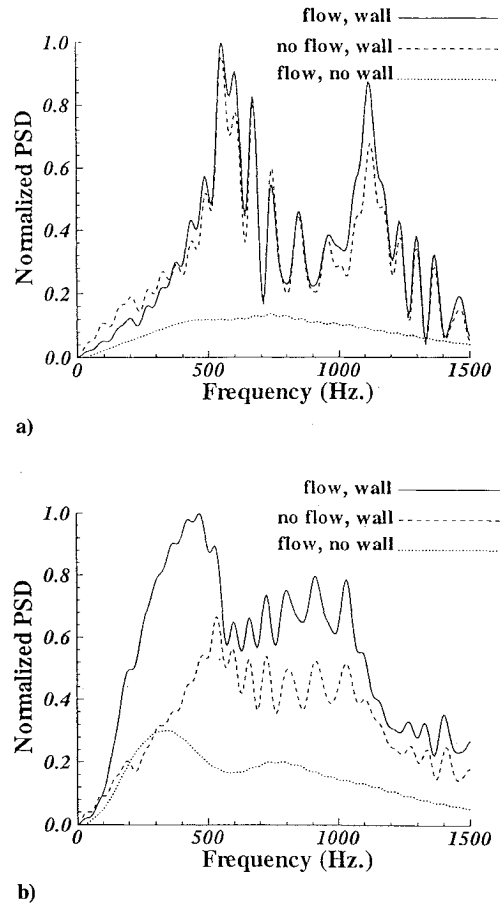

Fig. 7 PSD of incident $p - p_\infty$ for the computations of wall/flow, wall/no flow and no wall/flow: a) at the center of panel A and b) at the center of panel B.

We next consider the PSD (power spectral density) of the unsteady pressure p. We consider p at the centers of the two panels on both the jet side and the radiation side. On the jet side the total pressure field includes incident and reflected pressure as well as pressure radiated by the panels. On the radiation side the pressure is only that due to radiation by the panels. To clarify the mechanisms influencing the spectral content of p, we compare these results with those from two other computations. In the second computation we consider the same panel assembly and source, but with no flow. In this computation, the pressure disturbances on the bounding wall are due exclusively to the starter pulse. The third computation is of the jet flow only, without any bounding wall or panel assembly. Far-field results for this computation were shown in Fig. 3. The data on the jet side are presented in Figs. 7a and 7b for panels A and B, respectively. In each of these figures the data is normalized by the maximum (over all three computations) PSD at the considered location.

We note that for a rigid wall, the wall pressure will be doubled when compared to the pressure at the same location for the case without any wall. Since the PSD involves the square of the Fourier transform of p, the resulting PSD for the computations with the wall should be a factor of 4 greater than for comparable computations without any wall. In the present case there are additional effects due to radiation from the panels, but due to this geometric effect the PSD for the no-wall/flow computation should be roughly 25% of the PSD for the wall/flow and wall/no-flow computations. In analyzing the effects of flow and wall on the PSD, this purely geometrical effect should be taken into account.

Figure 7a shows that the PSDs of the incident pressure on panel A for the wall/flow computation are comprised of relatively discrete spectral bands. The behavior for the wall/no-flow computation exhibits similar discrete bands with lower amplitude levels. In contrast, the computation of no-wall/flow exhibits a continuous smooth spectrum. The discrete spectral bands exhibited for the wall/flow and wall/no-flow computations are a direct consequence of reflections between the wall and the nozzle and do not appear to be heavily influenced by the flow. The peak around 1000 Hz represents the peak frequency of the original pulse. The peak at around 500 Hz is due to reflections between the panel and the nozzle (requiring the disturbance to traverse a total distance of approximately 2 ft, since the pipe is located approximately 1 ft below the panel). We note that the no-wall/flow spectrum is similar to that shown in Fig. 3 which represents the same computation but with the pressure measured at 90 deg in the far field. This is a consequence of panel A being centered directly above the jet exit.

In contrast, the spectral data in Fig. 7b shows a much greater effect of the flow for panel B which is downstream of the jet exit. Both the wall/flow computation and the no-wall/flow computation exhibit a significant amplification of low frequencies as compared to the wall/no-flow computation (recall that for the no-wall/flow computation the overall level of the PSD is expected to be roughly 25% of the level for the wall/flow computation). This low-frequency amplification is attributed primarily to sound generated by instabilities within the flow. Note that the PSD of the no-wall/flow computation is similar to that of the far-field pressure at 30 deg (Fig. 3), a consequence of the fact that the center point of panel B is approximately 39 deg from the nozzle exit.

The wall/flow computation exhibits discrete spectral bands for higher frequencies. Similar discrete bands, although at a lower level, are also observed in the wall/no-flow computation. These bands appear to be induced by reflections between the wall and the pipe. These bands are not present without the wall. These bands are amplified due to the presence of the flow. Examination of panel velocities and radiated pressure (see next subsection) demonstrates that these higher frequency pressure disturbances do not excite significant panel response.

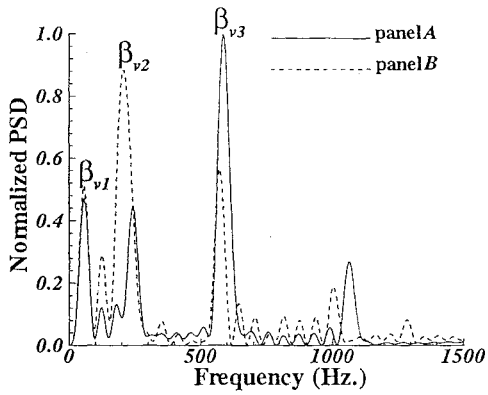

Fig. 8 PSD of v at panel centers.

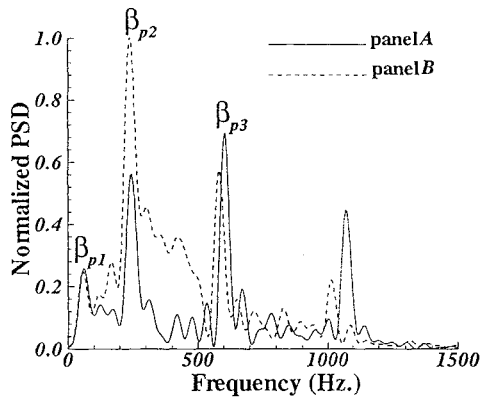

Fig. 9 PSD of transmitted pressure.

These results also demonstrate that the pressure along the walls and panels varies rapidly with downstream distance near the jet exit. Since the panels are identical in all respects, the loading on the panels depends very crucially on their location relative to the nozzle exit. Directional enhancement due to the flowfield as well as sound generated from instability waves are the primary mechanisms influencing panel excitation. The enhanced low-frequency loading on panel B, due to instability wave generated sound, is in a frequency band for which the panel can be readily excited. As will be seen, this enhanced loading is reflected in enhanced vibration of and radiation from panel B.

The effect of the enhanced low-frequency excitation of panel B can be seen in Figs. 8 and 9 where we plot the PSD for the panel velocities and radiated pressure, respectively, at the panel centers. Both panels exhibit relatively narrow, nearly coincident bands of low-frequency peak spectral response. We denote these bands for the velocity spectra by β_{v1}, β_{v2}, and β_{v3} and for the transmitted pressure spectra by β_{p1}, β_{p2}, and β_{p3}. We believe that the low-frequency bands are primarily due to convective modes along the panel. The reflections between panel A and the pipe should be manifested in higher frequencies. The enhanced low-frequency response of panel B is apparent from both figures. In view of the earlier analysis of the incident pressure, we attribute this enhanced response primarily to the instability wave generated sound which provides enhanced excitation of the downstream panel B.

We note that the broadband incident pressure on panel B is converted to a discrete velocity and transmitted pressure spectra. The three primary pressure bands, β_{p1}, β_{p2}, and β_{p3}, are clearly associated with the analogous velocity bands, β_{v1}, β_{v2}, and β_{v3}. The large response for panel B in the band β_{v2}, together with the associated radiation (β_{p2}), represent the main effect of the instability wave generated sound on the panels and reflects the frequencies within the broadband indicated in Fig. 7b at which the panel is most responsive. The higher frequency spectral bands observed in Figs. 7a and 7b do not excite significant panel response with the exception of the strong band around 1000 Hz for panel A which is near the peak of the original pulse.

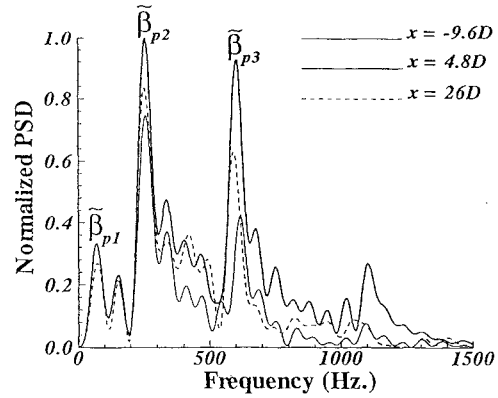

Fig. 10 PSD of radiated $p - p_\infty$ at $x = -12D, x = 6D, x = 18D$, along the line $y = 36D$.

The results indicate that panels located downstream of the jet exit act as narrow filters, converting a broadband forcing into relatively narrow spectral bands. The bands are concentrated in the low-frequency range, characteristic of instability wave generated sound, which indicates that shear layer instabilities can be an important mechanism in panel excitation.

D. Acoustic Radiation from the Panels

The time evolution of the pressure radiated by the motion of the panels is shown at successive times in Figs. 4a–4e. Figure 4a shows a nearly circular leading wave radiating away from the panels. This is due to the excitation of the panels by the leading acoustic disturbance initiated by the pulse starter. In addition, there is an asymmetrical disturbance generated primarily from panel B which propagates mainly in the downstream direction (Fig. 4b).

As time evolves, further radiation from both panels occurs. The figures clearly demonstrate a preferred downstream beaming of this radiation, although there is noticeable upstream acoustic propagation as well. This is in contrast to the nearly circular disturbance generated by the pulse starter. We note the presence of well-defined radiation even at late times, after the initial disturbance due to the pulse starter has exited the computational domain.

PSDs of the radiated pressure at sample far-field points are shown in Fig. 10. Results are presented along the line $y = 36D$ for selected values of x. The far-field spectra exhibit relatively discrete spectral bands. The three pronounced frequency and ($\tilde{\beta}_{p1}$, $\tilde{\beta}_{p2}$, and $\tilde{\beta}_{p3}$), are analogous to those for the velocity and transmitted pressure (Figs. 8 and 9). The primary feature of the radiation is the presence of the large peak ($\tilde{\beta}_{p2}$) near 250 Hz. This is an effect of the flow and, based on the transmitted pressure (for example, Fig. 9), is primarily due to radiation from the downstream panel (panel B). We note that although the panels can be most readily excited at low frequencies, the comparable peak in a computation with no flow is roughly three times larger than the peak indicated in Fig. 10. Thus, the low-frequency spike is a consequence of low-frequency sound generation and directional enhancement due to the flowfield.

IV. Conclusion

We have computed the full flow/acoustic/structure coupling for a model of a panel-stringer assembly forced by jet noise. The jet is initially excited by a pulse and continues radiating sound long after the initial disturbance due to the pulse has exited the computational domain, thus simulating the behavior of a real jet flowfield. We have computed directly the instability wave sources of sound in the jet as well as the resulting sound propagation and panel response and radiation. The instability wave sources generate directionally beamed low-frequency sound into the far field, primarily at low to midangles to the jet axis. Instability wave generated sound acts to excite the flexible panels, particularly the panel located downstream of the nozzle exit. The location of the panels with respect to the jet exit is critical in terms of the resulting structural vibration and acoustic radiation.

The response of panel B, located downstream of the jet exit, is primarily convective in nature, reflecting the primary forcing which is jet noise generated from the instability waves. The response of panel A, located directly above the nozzle exit, exhibits a combination of standing and convective waves, where the standing waves are induced by reflections between the pipe and the panel.

The panels act as a narrow filter, converting the relatively broadband incident pressure to a transmitted pressure exhibiting relatively narrow spectral bands. The narrow spectral bands are also present in the far-field radiation from the panels. The radiation from the panels is directed primarily downstream. Because of a continual excitation of instabilities in the jet, radiation persists long after the initial disturbance generated by the pulse exits the computational domain.

Acknowledgments

The first author was supported by NASA Langley Research Center, while in residence, under a National Research Council Postdoctoral Research Associateship Award. The second author was partially supported by NASA Langley Research Center under Contracts NAS1-18605 and NAS1-19480 while in residence at the Institute for Computer Applications in Science and Engineering. The authors thank Jay Hardin for helpful discussions and comments.

References

[1]Lighthill, M. J., "On Sound Generated Aerodynamically—II, General Theory," *Proceedings of the Royal Society*, Vol. A222, Ser. A, 1954, pp. 1–32.

[2]Ribner, H. S., "Dryden Lecture Perspectives on Jet Noise," *AIAA Journal*, Vol. 19, Dec. 1981, pp. 1513–1526.

[3]Lilly, G. M., "Theory of Turbulance Generated Jet Noise: Generation of Sound in a Mixing Region," Air Force Aero Propulsion Lab., U. S. Air Force Technical Rept. AFAPL-TR-72-53, IV, Wright Patterson AFB, 1972.

[4]Phillips, O. M., "The Irrotational Motion Outside the Free Turbulent Boundary," *Proceedings of the Cambridge Philosophical Society*, Vol. 51, 1955, pp. 222–229.

[5]Ting L., and Miksis, M. J., "On Vortical Flow and Sound Generation," *Journal of Applied Mathematics*, Vol. 50, 1990, pp. 521–536.

[6]Crow, S., and Champagne, F., "Orderly Structure in Jet Turbulence," *Journal of Fluid Mechanics*, Vol. 48, Aug. 1971, pp. 457–591.

[7]Kibens, V., "Discrete Noise Spectrum Generated by an Acoustically Excited Jet," *AIAA Journal*, Vol. 18, April 1980, pp. 434–441.

[8]Maestrello, L., Bayliss, A., and Turkel, E., "On the Interaction of a Sound Pulse with the Shear Layer of an Axisymmetric Jet," *Journal of Sound and Vibration*, Vol. 74, 1981, pp. 281–301.

[9]Vlasov, Y. V., and Ginevsky, A. S., "Generation and Supprsession of Turbulence in an Axisymmetric Turbulent Jet in the Presence of an Acoustic Influence," NASA-TT-F15721, June 1974, p. 721.

[10]Bechert, D. W., and Pfizenmaier, E., "On the Amplification of Broadband Jet Noise by Pure Tone Excitation," *Journal of Sound and Vibration*, Vol. 43, 1975, pp. 581–587.

[11]Huerre, P., and Monkewitz, P. A., "Absolute and Convective Instabilities in Shear Layers," *Journal of Fluid Mechanics*, Vol. 159, Oct. 1985, pp. 151–168.

[12]Huerre, P., and Monkewitz, P. A., "Local and Global Instabilities in Spatially-Developing Flows," *Annual Review of Fluid Mechanics*, Vol. 22, 1990, pp. 473–537.

[13]Michalke, A., and Hermann, G., "On the Inviscid Instability of a Circular Jet With External Flow," *Journal of Fluid Mechanics*, Vol. 114, 1982, pp. 343–359.

[14]Michalke, A., "Survey on Jet Instability Theory," *Progress in Aerospace Science*, Vol. 21, No. 3, 1984, pp. 159–199.

[15]Tam, C. K. W., "Jet Noise Generated by Large-Scale Coherent Motion," *Aeroacoustics of Flight Vehicles, Theory and Practice*, edited by H. H. Hubbard, NASA, WRDC, TR 90-3052, Vol. 1, 1991, Chap. 6.

[16]Bayliss, A., Maestrello, L., and Turkel, E., "On the Interaction of a Sound Pulse With the Shear Layer of an Axisymmetric Jet, III: Non-Linear Effects," *Journal of Sound and Vibration*, Vol. 107, 1986, pp. 167–175.

[17]Maestrello, L., and Bayliss, A., "Flowfield and Far Field Acoustic Amplification Properties of Heated and Unheated Jets," *AIAA Journal*, Vol. 20, Nov. 1982, pp. 1539–1546.

[18]Mankbadi, R., Hayder, M., and Povinelli, L., "The Structure of Supersonic Jet Flow and Its Radiated Sound," AIAA Paper 93-0549, Jan. 1993.

[19]Dowell, E. H., "Transmission of Noise from a Turbulent Boundary Layer through a Flexible Plate into a Closed Cavity," *Journal of the Acoustic Society of America*, Vol. 46, 1969, pp. 238–252.

[20]Maestrello, L., and Pao, S. P., "New Evidence of the Mechanisms of Noise Generation and Radiation of a Subsonic Jet," *Journal of the Acoustical Society of America*, Vol. 57, No. 4, 1975, pp. 959, 960.

[21]Blevins, R. D., "An Approximate Method for Sonic Fatigue Analysis of Plates and Shells," *Journal of Sound and Vibration*, Vol. 129, 1989, pp. 51–71.

[22]Wang, T., "Dynamic Forcing Function for Flow-Acoustic-Induced Vibration," *Journal of Pressure Vessel Technology*, Vol. 111, 1989, pp. 361–370.

[23]Maestrello, L., "Active Control of Nonlinear-Nonstationary Response and Radiation of a Panel-Stringer Structure Near a Supersonic Jet," AIAA Paper 93-4338, Oct. 1993.

[24]Hoff, C., and Pahl, P. J., "Development of an Implicit Method With Numerical Dissipation From a Generalized Single-Step Algorithm for Structural Dynamics," *Computer Methods in Applied Mechanics and Engineering 67*, North-Holland, Amsterdam, 1988, pp. 367–385.

[25]Maestrello, L., "Acoustic Energy Flow From Subsonic Jets and Their Mean and Turbulent Flow Structure," Ph.D. Thesis, Univ. of Southampton, England, UK, 1975.

[26]Bayliss, A., and Turkel, E., "Far-Field Boundary Conditions For Compressible Flows," *Journal of Computational Physics*, Vol. 48, 1982, pp. 182–199.

[27]Gottlieb, D., and Turkel, E., "Dissipative Two-Four Methods For Time-Dependent Problems," *Mathematic Computation*, Vol. 30, 1976, pp. 703–723.

[28]Bayliss, A., Parikh, P., Maestrello, L., and Turkel, E., "A Fourth Order Scheme For the Unsteady Compressible Navier–Stokes Equations," AIAA Paper 85-1694, July 1985.

[29]Bayliss, A., and Maestrello, L., "Simulation of Instabilities and Sound Radiation in a Jet," *AIAA Journal*, Vol. 19, July 1981, pp. 835–841.

[30]Ho, C. M., and Huang, L. S., "Subharmonics and Vortex Merging in Mixing Layers," *Journal of Fluid Mechanics*, Vol. 119, 1982, pp. 443–473.